学位論文

「**RAMP1 signaling in immune cells regulates inflammation-associated lymphangiogenesis** 」
（免疫細胞における RAMP1 シグナルの腹膜炎時リンパ管新生制御に果たす役割について）

ＤＭ１４０１５　津留　世里

北里大学大学院医療系研究科医学専攻博士課程
麻酔科
指導教授　岡本　浩嗣

著者の宣言

本学位論文は、著者の責任において実験を遂行し、得られた真実の結果に基づいて正確に作成したものに相違ないことをここに宣言する。

Abstract

Objective Calcitonin gene-related peptide (CGRP) regulates inflammation via signaling through receptor activity-modifying protein (RAMP) 1, a subunit of the CGRP receptor. Here, we investigated the role of RAMP1 signaling in growth of lymphatic vessels during inflammation.

Approach and Results Lymphangiogenesis in the diaphragm of RAMP1-deficient ($^{-/-}$) mice or their wild-type (WT) counterparts was induced by repeated intraperitoneal injection of lipopolysaccharide (LPS). Compared with WT mice, LPS-induced lymphangiogenesis in diaphragm tissues from RAMP1$^{-/-}$ mice was suppressed. This was accompanied by reduced expression of vascular endothelial growth factor (VEGF)-C and VEGF-D. The number of $CD4^+$ cells in WT mice was greater than that in RAMP1$^{-/-}$ mice. Removing $CD4^+$ cells attenuated lymphangiogenesis and expression of VEGF-C and VEGF-D. $CD4^+$ cells isolated from RAMP1$^{-/-}$ mice exhibited reduced expression of VEGF-C and VEGF-D. The number of $CD11b^+$ cells in RAMP1$^{-/-}$ mice was higher than that in WT mice and was associated with upregulated expression of genes related to pro-inflammatory macrophages and downregulation of restorative macrophage-related expression. Bone marrow cells expressing RAMP1 showed increased lymphangiogenesis. When fluorescein isothiocyanate (FITC)-dextran was injected into the peritoneal cavity of WT mice, the amount of residual FITC-dextran was lower than that in RAMP1$^{-/-}$ mice.

Conclusions The present results suggest that RAMP1 signaling in immune cells plays a critical role in inflammation-related lymphangiogenesis; therefore, it represents a novel target for controlling lymphangiogenesis.

目次

1. Introduction

Calcitonin gene-related peptide (CGRP) is a 37 amino acid neuropeptide distributed widely in both the central and peripheral nervous systems [1,2]. The functional CGRP receptor is a heterodimer comprising a seven-transmembrane G protein, calcitonin receptor-like receptor (CLR) and a single membrane-spanning protein, receptor activity-modifying protein (RAMP) 1 [3,4]. Because RAMP1 is required for CGRP binding to CLR [5], it is suggested that RAMP1 is rate limiting not only for cAMP generation, but also for downstream effects on the intracellular signaling in CLR [6,7]. RAMP1 is also activated by amylin, which is a 37 amino acid peptide hormone that is about 50% identical to CGRP [8]. Release of CGRP from unmyelinated C fibers occurs during neuroinflammation. The nervous system regulates both immune homeostasis and inflammation; the significance of crosstalk between the nervous and immune systems with respect to disease course is increasingly apparent [9]. Previously, we showed that RAMP1 signaling in immune cells, including macrophages and T cells, is important for suppression of inflammation in the intestine and liver [10,11,12].

Lymphatic vessels play an essential role in maintaining tissue fluid homeostasis by regulating uptake of interstitial fluid into draining lymphatic vessels and transport of the drained lymphatic fluid to the blood vasculature via collecting lymphatic vessels. The lymphatic system and the immune system are intimately connected; indeed, recent studies show that lymphatic vessels are dynamic structures that react to inflammatory stimuli [13]. Inflammation-associated formation of new lymphatics, i.e., lymphangiogenesis, is not only an endpoint of inflammation, but also a phenomenon actively involved in the pathophysiology of various inflammatory conditions [14]. Indeed, lymphangiogenesis has functional consequences not only for lymphatic transport, but also for inflammation resolution and tissue repair [14,15,16]. Previously, we showed that lymphangiogenesis in granulation tissues during wound healing is enhanced by the endogenous CGRP/RAMP1 pathway [17]. We also demonstrated that RAMP1 signaling plays a role in lymphangiogenesis during secondary lymphedema [18].

Diaphragmatic lymphatic vessels represent a central route for drainage of peritoneal fluid [19,20,21]; these vessels drain molecules and fluid to the mediastinal lymph nodes [22]. The lymphatic vessels in the diaphragm are well developed and so are easily studied in adult mice [21]. However, it remains unknown whether RAMP1 signaling increases lymphangiogenesis in diaphragm tissues during inflammation. Here, we used a mouse model to examine the role of RAMP1 signaling in inflammation-associated lymphangiogenesis elicited by intraperitoneal injection of lipopolysaccharide (LPS).

2. Materials and methods

2-1. Animals and treatment

Male RAMP1-deficient (RAMP1$^{-/-}$) mice (8–10 weeks old) were generated as described elsewhere [10]. Male C57BL/6 mice (8–10 weeks old) were obtained from Clea Japan (Tokyo, Japan) and used as controls. Knockout mice were backcrossed to the C57BL/6 background for more than ten generations. Mice ubiquitously expressing green fluorescent protein (GFP) were kindly provided by Dr. Okabe (Genome Information Research Center, Osaka University, Osaka, Japan) and housed at Kitasato University under specific pathogen-free conditions. Mice were maintained at constant humidity (60% ± 5%) and temperature (25°C ± 1°C) on a 12 h light/dark cycle. All animals were provided with food and water *ad libitum*. All experimental procedures were approved by the Animal Experimentation and Ethics Committee of the Kitasato University School of Medicine (2017-124) and were performed in accordance with the guidelines for animal experiments set down by the Kitasato University School of Medicine, which are in accordance with the "Guidelines for Proper Conduct of Animal Experiments" published by the Science Council of Japan. Peritonitis was induced by peritoneal injection of LPS (Sigma, E coli, 0111-B4; Sigma-Aldrich, St. Louis, MO, USA) (1 μg/g of body weight) in 200 μl of PBS (injections were performed every other day, starting at the beginning of the experiment). As a control, 200 μl of PBS was injected in the same manner. We defined Day 0 as day at the beginning of the experiment just prior to the first LPS administration, and Day 1 as 1 day after the start of the first LPS administration.

2-2. Depletion of CD4$^+$ T cells

Experimental animals were depleted of CD4$^+$ cells using a rat anti-mouse CD4 monoclonal IgG2b antibody (clone GK1.5; BioLegend, San Diego, CA, USA). The antibody was administered i.p. (300 μg per mouse) 24 h before LPS administration, as described previously [8]. Control animals were treated with an IgG isotype control antibody (BioLegend).

2-3. Real-time RT-PCR

Transcripts encoding CGRP, Pro-CGRP, RAMP1, Lyve-1, VEGFR3, Prox-1, VEGF-C, VEGF-D, TNFα, mannose receptor (MR), CCL2, CCL5, and glyceraldehyde-3-phosphate dehydrogenase (GAPDH) were quantified by real-time RT-PCR analysis. Total RNA was extracted from mouse tissues and homogenized in TRIzol reagent (Life Technologies, Carlsbad, CA, USA). Single-stranded cDNA was generated from 1 μg of total RNA via reverse transcription using the ReverTra Ace® qPCR RT Kit (TOYOBO Co., Ltd., Osaka, Japan), according to the manufacturer's instructions. Quantitative PCR amplification was performed using SYBR Premix Ex Taq™ II (Tli RNaseH Plus; Takara Bio, Inc. Shiga, Japan). The gene-specific primers used for real-time RT-PCR were designed using Primer 3

software (http://primer3.sourceforge.net/) based on data from GenBank. The primers are described in Supplementary Table 1.

2-4. Expression of pro-CGRP, CGRP, and RAMP1 in dorsal root ganglions (DRGs)

The medulla spinalis was removed, and the DRGs of the C_{3-6} vertebrae were isolated. DRG tissues were homogenized in 1 ml of TRIzol reagent (Life Technologies). A sample of RNA was extracted from the tissue according to the manufacturer's instructions. Real-time PCR was performed as described above.

2-5. Drainage of FITC-dextran from the peritoneal cavity

For the dye efflux experiment, 1 ml of 0.2% FITC-dextran (MW 2,000,000, Sigma) was injected into the peritoneal cavity of mice using a micro syringe. Under anesthesia with isoflurane, mice were sacrificed after 10 min and any FITC-dextran remaining in the peritoneal cavity was extracted with 5 ml of PBS. Immediately after collecting peritoneal fluid, the thoracic cavity was opened. The right mediastinal lymph nodes were removed and placed into vials filled with 50 μl of PBS. To estimate the amount of drainage, the fluorescence intensity of the lavage fluid and mediastinal lymph nodes was measured using a Thermo Scientific NanoDrop 3300 (Fluorospectrometer) with an excitation wavelength of 495 nm and an emission wavelength of 519 nm.

2-6. Determination of intraperitoneal pressure

In separate experiments, mice were anesthetized by intraperitoneal (i.p.) injection of a mixture of medetomidine hydrochloride (0.75 mg/kg) (Nippon Zenyaku Kogyo Co., Ltd., Fukushima, Japan), midazolam (4.0 mg/kg) (Astellas Pharma Inc., Tokyo, Japan), and butorphanol (5.0 mg/kg) (Meiji Seika Pharma Co., Ltd., Tokyo, Japan) [23]. The intraperitoneal pressure was determined with a 25G needle which inserted via the left lower abdomen, connected to a pressure during the continuous infusion of saline with a 24G needle inserted through the right lower abdomen. Saline was continuously infused at 2 ml/min, and pressure was recorded using a data acquisition system (PowerLab/8SP; AD Instruments. Colorado Springs, CO, USA). The data were analyzed using the PowerLab Chart 5 software (PowerLab; AD Instruments).

2-7. Immunofluorescence analysis

On the indicated days after treatment, mice were anesthetized with isoflurane and the diaphragm was harvested. Whole-mounted diaphragm tissues were fixed with 4% paraformaldehyde in PBS, followed by incubation for 60 min in cold PBS containing 2% H_2O_2 and then for 1 h in cold PBST (0.5% Triton X-100 in PBS). After blocking, sections were incubated overnight at 4°C with a rabbit anti-mouse RAMP1 polyclonal antibody (Santa Cruz Biotechnology, CA, USA), a rat anti-mouse CD4

monoclonal antibody (eBioscience, San Diego, CA, USA), a rabbit anti-mouse CD11b monoclonal antibody (Abcam, Cambridge, MA, USA), anti-VEGF-C (E-6, mouse monoclonal antibody; Santa Cruz Biotechnology, CA, USA), anti-VEGF-D (C-12, mouse monoclonal antibody; Santa Cruz Biotechnology, CA, USA), or a rabbit anti-mouse Lyve-1 polyclonal antibody (Abcam). After washing three times in PBS, the sections were incubated for 1 h at room temperature with a mixture of the following secondary antibodies: Alexa Fluor® 594-conjugated donkey anti-rat IgG, Alexa Fluor® 488-conjugated donkey anti-rabbit IgG, Alexa Fluor® 488-conjugated donkey anti-goat IgG (all from Molecular Probes, OR, USA), and Alexa Fluor® 594-conjugated goat anti-guinea pig IgG (Abcam). These antibodies were diluted in Antibody Diluent with Background-Reducing Components (Agilent, CA, USA). Images were observed and captured under a confocal scanning laser microscope (LSM710; Carl Zeiss, Jena, Germany) or a fluorescence microscope (Biozero BZ-9000 Series; KEYENCE, Osaka, Japan). After labeling, ten low-power optical fields (40× magnification) were randomly selected and the number of positive cells was counted. The results were expressed as the average number of positive cells per field. Lymphatic microvessels in the diaphragm (a parameter of lymphangiogenesis) were assessed using ImageJ software. The Lyve-1^+ area was calculated, and the results were expressed as the percentage of lymphatic microvessel area (LVA%).

2-8. Isolation of lymphocytes from spleen and blood

Mice were anesthetized with pentobarbital sodium solution (75 mg/kg, i.p.), and the spleen was collected and placed immediately in ice-cold RPMI. The tissue was pressed through a 70 μm cell strainer, and erythrocytes were disrupted in lysis buffer. Viable, nucleated cells were counted by trypan blue exclusion. Blood samples from the heart were collected. The white blood cells were separated on Lymphosepar II (Immuno-Biological Laboratories, Gunma, Japan).

2-9. $CD4^+$ T cells culture

$CD4^+$ cells were isolated from the spleen using the mouse $CD4^+$ T cell Isolation Kit (Miltenyi Biotec, Auburn, CA, USA), according to the manufacturer's instructions. Isolated $CD4^+$ cells (10^6 cells/ml) were stimulated with 1 mg/ml anti-CD3 (BioLegend) and 1 mg/ml anti-CD28 (BioLegend). After 24 h, cells were stimulated for 3 h with LPS with or without CGRP (10nM) (Peptide Institute, Inc., Osaka, Japan) in RPMI 1640 medium. $CD4^+$ T cells were then
harvested and homogenized in TRIzol (Life Technologies), and mRNA levels were measured by real-time RT-PCR.

2-10. Flow cytometry analysis

Cells were incubated with the 2.4G2 mAb (anti-cγRIII/II) to block non-specific binding of the primary mAb. Then, cells were stained with a combination of the following fluorochrome-conjugated

antibodies: anti-CD3 (clone 17A2, BioLegend) and anti-CD4 (clone GK1.5, BioLegend). Tubes were placed in the dark on ice for 30 min. Pellets were washed twice with PBS. Samples were measured on a FACSVerse™ (BD, Franklin Lakes, NJ, USA). The data were analyzed using Kaluza software v1.3 (Beckman Coulter, Brea, CA, USA) [12].

2-11. Isolation of macrophages from the bone marrow (BM)

BM cells were isolated from the femur and tibia of 12-week-old WT and RAMP1$^{-/-}$ mice. Femurs and tibias were flushed with PBS, and erythrocytes were lysed by treatment with RBC lysis buffer (BioLegend). To generate BM-derived macrophages, BM cells were cultured in RPMI 1640 medium containing 10% fetal calf serum and macrophage colony stimulating factor (M-CSF) (20 ng/ml; BioLegend) and plated in 6-well plates (1.0×10^6 cells per well). On Day 7, cells stimulated with LPS (100 ng/ml, Sigma) were treated (or not) for 3 h with CGRP (10 nM) (Peptide Institute) in RPMI 1640 medium. BM-derived macrophages were then harvested and homogenized in TRIzol (Life Technologies), and mRNA levels were measured by real-time RT-PCR.

2-12. Murine BM transplantation model

BM transplantation was performed as previously described [19]. Briefly, recipient mice were treated with clodronate-loaded liposomes (200 μl/mouse; FormuMax Scientific, Inc., Palo Alto, CA, USA) to deplete tissue macrophages at 48 h before irradiation. Donor BM cells from RAMP1$^{-/-}$ mice and their WT counterparts were harvested using the same method. Mice were irradiated in a MBR-1505R X-ray irradiator (9.5 Gy; Hitachi Medical Co., Tokyo, Japan) with a filter (copper, 0.5 mm; aluminum, 2 mm) while the cumulative radiation dose was monitored. Donor BM-derived mononuclear cells (1×10^7 cells/200 μl of PBS) were injected into the tail vein of irradiated mice.

2-13. Statistical analysis

All results are expressed as the mean ± SD. All statistical analyses were performed using GraphPad Prism software, version 8 (GraphPad Software, La Jolla, CA, USA). An unpaired
two-tailed Student's t-test was used to compare data between two groups. One-way analysis of variance, followed by Turkey's post-hoc test, was used to compare data between multiple groups. A p-value < 0.05 was considered statistically significant.

3. Results

3-1. RAMP1$^{-/-}$ mice show suppression of lymphangiogenesis and expression of genes encoding lymphangiogenic factors

Injection of LPS into the peritoneal cavity of WT mice led to increased lymphangiogenesis, as indicated by a gradual and significant increase in LVA% in the diaphragm compared with that in vehicle (PBS)-treated WT mice (Supplementary Fig. 1a, b). Lymphangiogenesis in LPS-treated mice peaked at Days 7 and 14. Based on these results, we examined inflammation-associated lymphangiogenesis up until Day 7 in all subsequent experiments.

Next, we determined the functional role of RAMP1 signaling during lymphangiogenesis. There was no significant difference in basal LVA% between WT and RAMP1$^{-/-}$ mice. At Days 5 and 7, LVA% in the diaphragm of WT mice receiving i.p. injection of LPS into the peritoneal cavity was higher than that in RAMP1$^{-/-}$ mice (Fig. 1a, b). These results suggest that RAMP1 signaling facilitates inflammation-associated lymphangiogenesis.

At Days 5 and 7, levels of mRNA encoding Lyve-1, VEGFR3, and Prox-1 (markers of lymphatic endothelial cells) in the diaphragm were higher in LPS-treated WT mice than in LPS-treated RAMP1$^{-/-}$ mice (Fig. 1c-e). Expression of pro-lymphangiogenic factors VEGF-C and VEGF-D was also higher in LPS-treated WT mice on Day 5 and Days 3 and 5, respectively, than in LPS-treated RAMP1$^{-/-}$ mice (Fig. 1f, g). Collectively, these results suggest that RAMP1 signaling promotes lymphangiogenesis by inducing expression of VEGF-C and VEGF-D.

3-2. Expression of RAMP1 in the DRG and diaphragm tissues

Basal levels of mRNA encoding pro-CGRP and CGRP in cervical DRG tissues from non-treated RAMP1$^{-/-}$ mice were no different from those in WT mice (Supplementary Fig. 2a, b), suggesting that CGRP levels in the neuronal system were not reduced in RAMP1$^{-/-}$ mice. By contrast, RAMP1 expression in DRGs from RAMP1$^{-/-}$ mice was much lower than that in DRGs from WT mice (Supplementary Fig. 2c). These results suggest that RAMP1$^{-/-}$ mice are good tools for evaluating CGRP signaling under pathologic conditions.

Therefore, to examine localization of RAMP1 expression in lymphatic endothelial cells in the diaphragm, we performed double immunostaining for RAMP1 and Lyve-1 (Supplementary Fig. 2d). No RAMP1/Lyve-1 double-positive vessels were observed in diaphragm tissues at Day 0 (day at the beginning of the experiment just prior to the first LPS administration) and Day 7 (7 days after the

start of the first LPS administration), indicating that newly formed lymphatic vessels do not express RAMP1. These results suggest that CGRP/RAMP1 signaling does not affect newly formed lymphatic vessels directly. In addition, immunofluorescence analysis revealed that RAMP1 co-localized with $CD4^+$ cells (Supplementary Fig. 2e) as well as with $CD11b^+$ cells (Supplementary Fig. 2f), indicating that T cells and macrophages express RAMP1.

3-3. Accumulation of T cells and macrophages in the diaphragm

Because T cells and macrophages play roles in inflammatory-associated lymphangiogenesis in the diaphragm [16,18], we counted the number of T cells and macrophages in diaphragm tissue from mice with LPS-induced peritonitis (Fig. 2a, b). Immunofluorescence analysis revealed that the number of $CD4^+$ cells (T cells) in WT mice at Day 3 was larger than that in $RAMP1^{-/-}$ mice (Fig. 2b). Accumulation of $CD4^+$ cells in WT mice tended to be higher at Day 7; however, the difference did not reach statistical significance.

We also counted the number of $CD11b^+$ cells (macrophages) in the diaphragm (Fig. 2c). The number of $CD11b^+$ cells in the diaphragm of LPS-induced WT mice at Day 3 was higher than that at Day 0, and numbers were even higher in $RAMP1^{-/-}$ mice. At Day 7, there was no significant difference in $CD11b^+$ cell numbers between the genotypes. These results suggest that accumulation of $CD4^+$ cells (T cells) and $CD11b^+$ cells (macrophages) was correlated with lymphangiogenesis.

To examine whether T cells and macrophages express lymphangiogenic factors, we performed immunostaining of diaphragm tissue to detect immune cells and VEGF-C or VEGF-D (Fig. 2d, e). On Day 3, diaphragm tissue from LPS-induced WT mice contained $CD4^+$ cells that were positive for VEGF-C and VEGF-D (Fig. 2d). The percentages of VEGF-C and VEGF-D expression in $CD4^+$ cells were approximately 70% or 90%, respectively (Fig. 2d). The same was true for diaphragm tissue subjected to double immunostaining with antibodies specific for CD11b, VEGF-C, or VEGF-D. $CD11b^+$ cells were positive for both VEGF-C and VEGF-D (Fig. 2e). The approximately 80% of $CD11b^+$ cells were positive for VEGF-C or VEGF-D (Fig. 2e).

3-4. T cells contribute to lymphangiogenesis during inflammation

To further examine the involvement of $CD4^+$ T cells in lymphangiogenesis, $CD4^+$ T cells were deleted from the circulation of mice by injection of anti-CD4 or isotype IgG antibodies prior to injection of LPS. Treatment with anti-CD4 neutralizing antibodies significantly reduced the percentages of $CD4^+$

cells in the blood and spleen from WT and RAMP1$^{-/-}$ mice as compared with control IgG (Supplementary Fig. 3). Treatment of WT mice with anti-CD4 antibodies led to marked suppression of lymphangiogenesis, as evidenced by reduction in both LVA% and expression of genes encoding VEGF-C and VEGF-D (Fig. 3a–d). In addition, LVA% and expression of VEGF-C and VEGF-D in RAMP1$^{-/-}$ mice treated with an anti-CD4 antibody did not differ from those in RAMP1$^{-/-}$ mice treated with the isotype control IgG antibody (Fig. 3b-d).

To determine whether CGRP/RAMP1 signaling regulates expression of VEGF-C and VEGF-D in CD4^{+} T cells, we isolated splenic CD4^{+} cells from WT and RAMP1$^{-/-}$ mice and exposed them to CGRP. CGRP increased expression of mRNA encoding VEGF-C and VEGF-D in WT CD4^{+} T cells; by contrast, expression was downregulated in RAMP1-deficient CD4^{+} T cells (Fig. 3e, f). These results indicate that CD4^{+} cells play an important role in LPS-induced lymphangiogenesis in diaphragm tissues by inducing expression of VEGF-C and VEGF-D.

3-5. Macrophages suppress lymphangiogenesis in RAMP1$^{-/-}$ mice

Macrophages also play a role in lymphangiogenesis in diaphragm tissues in response to LPS [16,18]. However, accumulation of macrophages in RAMP1$^{-/-}$ mice suppressed lymphangiogenesis (Fig. 1b, 2c). These results suggest that RAMP1 deficiency would affect the profiles of macrophages accumulating in the diaphragm of LPS-treated mice. When expression of genes encoding pro-inflammatory cytokines was measured by real-time RT-PCR, we found that expression of mRNA encoding TNFα in RAMP1$^{-/-}$ mice was higher than that in WT mice (Fig. 4a), whereas expression of mRNA encoding MR was lower than that in WT mice (Fig. 4b). Enhanced accumulation of macrophages in RAMP1$^{-/-}$ mice was associated with upregulated expression of chemokines, including CCL2 and CCL5 (Fig. 4c, d). These results suggest that inflammatory macrophages are recruited to the diaphragm in RAMP1$^{-/-}$ mice.

Additionally, *in vitro* experiments showed that TNFα expression by macrophages isolated from the BM of WT mice was downregulated in response to CGRP (Fig. 5a). By contrast, expression in macrophages isolated from RAMP1$^{-/-}$ mice was unchanged. However, expression of genes encoding MR in macrophages from WT mice was higher than that in RAMP1$^{-/-}$ mice (Fig. 5b). Furthermore, CGRP-mediated expression of VEGF-C in WT macrophages was higher than that in RAMP1$^{-/-}$ macrophages, whereas there was no significant difference in VEGF-D expression by macrophages from WT and RAMP1$^{-/-}$ mice (Fig. 5c, d). These results suggest that RAMP1 signaling upregulates lymphangiogenesis in the diaphragm by inducing expression of VEGF-C in macrophages.

Next, we examined the role of RAMP1-expressing BM cells in lymphangiogenesis. Compared with WT mice transplanted with WT-BM cells, WT mice bearing RAMP1-deficient BM cells showed a marked reduction in lymphangiogenesis (Supplementary Fig. 4a, b). On Day 7, GFP^+ cells accumulated in the diaphragm of WT mice receiving BM cells from GFP-transgenic mice (Supplementary Fig. 4c, d), suggesting that transplanted BM cells were recruited to the diaphragm. Double immunostaining analysis revealed that expression of GFP co-localized with that of CD11b, but not with that of CD4 (Supplementary Fig. 4c, d), indicating that the recruited BM cells were macrophages. Collectively, these results suggest that BM-derived macrophages expressing RAMP1 are recruited to the inflamed diaphragm, where they appear to secrete VEGF-C in response to CGRP stimulation, thereby contributing to lymphangiogenesis.

3-6. Drainage from the peritoneal cavity through lymphatic vessels in the diaphragm

We determined whether the injected volumes affected the intraperitoneal pressure. The intraperitoneal pressures remained unchanged up to total 8 ml injection of saline in both of WT and $RAMP1^{-/-}$ mice treated with LPS for 7 days (Supplementary Figure 5). The collected volumes of intraperitoneal fluids in WT and $RAMP1^{-/-}$ mice were 4.0 ± 0.2 mL and 4.2 ± 0.2 mL, respectively (n=5 per group). There was no statistical difference in the pressures between the genotypes. To compare the drainage function of lymphatic vessels in the diaphragm, we injected FITC-dextran into the peritoneal cavity and measured the amount of residual material 10 min after FITC-dextran injection. The amount of residual FITC-dextran in WT mice treated with LPS was lower than that in mice treated with vehicle (Fig. 6a). By contrast, the amount of residual FITC in LPS-treated $RAMP1^{-/-}$ mice was no different from that in vehicle-treated $RAMP1^{-/-}$ mice (Fig. 6a). These results suggest that lymphatic drainage of peritoneal fluid is hampered in $RAMP1^{-/-}$ mice. The lymphatic fluid in the diaphragm drains into the mediastinal lymphatic nodes. To further examine the drainage capacity of the lymphatic vessels in diaphragm tissue, we collected the right mediastinal lymphatic nodes and measured the fluorescence intensity of FITC-dextran (Figure 6b). The amount of FITC-dextran in the right mediastinal lymphatic nodes from WT mice was higher than that in those from $RAMP1^{-/-}$ mice (Fig. 6c). These results indicate that RAMP1 signaling improves the drainage function of lymphatic vessels in the diaphragm of mice with peritonitis. Taken together, lymphatic vessels in the diaphragm have an important functional role in draining interstitial fluid from the peritoneal cavity.

4. Discussion

The neuropeptide CGRP has anti-inflammatory effects on immune cells, including macrophages [12], T cells [25], and dendritic cells [26], through RAMP1 signaling. CGRP, which is produced in the nervous system, plays a role in growth of blood vessels under pathological conditions. Previously, we reported that CGRP plays a role in pathological angiogenesis by inducing a potent proangiogenic growth factor known as VEGF-A [27,28,29]. CGRP induced proliferation of human umbilical vein endothelial cells *in vitro* [27]. In addition, the CGRP/RAMP1 axis promotes angiogenesis during tumor growth [28] and tissue repair after gastric ulcers and hind-limb ischemia in mice [27,29]. In contrast to angiogenesis, little is known about RAMP1-induced lymphangiogenesis during inflammation.

Lymphatic vessels formed in response to inflammation are regulated by pro-lymphangiogenic factors (VEGF-C and VEGF-D) secreted by immune cells [15]. We hypothesized that RAMP1 signaling mediates lymphangiogenesis in diaphragm tissue during inflammation by affecting the function of immune cells. Here, we demonstrate that genetic deletion of RAMP1 signaling suppresses lymphangiogenesis in diaphragm tissue during development of LPS-induced peritonitis by reducing expression of VEGF-C and VEGF-D. Impaired lymphangiogenesis induced by RAMP1 deficiency was associated with reduced recruitment of $CD4^+$ T cells and increased recruitment of pro-inflammatory macrophages to the diaphragm. Furthermore, $RAMP1^{-/-}$ mice showed disrupted drainage of peritoneal fluid. These results indicate that RAMP1 signaling in immune cells promotes lymphangiogenesis and enhances drainage of peritoneal fluid.

The present study shows that T cells play roles in lymphangiogenesis in inflamed diaphragm tissue, which is in agreement with our previous study [20]. $CD4^+$ T cells contribute to lymphangiogenesis; indeed, depletion of $CD4^+$ T cells attenuates development of lymphedema in mice [25]. Here, we used a peritonitis model to show that $CD4^+$ T cells accumulate in the inflamed diaphragm. Accumulation of $CD4^+$ T cells expressing RAMP1 is positively associated with lymphangiogenesis. Deletion of $CD4^+$ T cells by injection of neutralizing antibodies suppressed lymphangiogenesis in the diaphragm of WT mice, but did not further attenuate lymphangiogenesis in $RAMP1^{-/-}$ mice, suggesting that $CD4^+$ T cells expressing RAMP1 play a critical role in accelerating lymphangiogenesis. T cells also could be a source of pro-lymphangiogenic cytokines [20,30]. *In vitro* experiments revealed that expression of VEGF-C and VEGF-D in $CD4^+$ T cells increased in a RAMP1-dependent manner. Collectively, the data suggest that RAMP1 signaling in $CD4^+$ T cells contributes to induction of inflammation-related lymphangiogenesis by increasing expression of VEGF-C and VEGF-D. Activation of the CGRP receptor results in activation of adenylate cyclase, which causes accumulation of cyclic AMP in

endothelial cells, vascular smooth muscle cells, and inflammatory cells [31]. Accumulation of cAMP upregulates expression of VEGF [32]. In addition, accumulation of cAMP upregulates cyclic AMP–responsive element binding protein (CREB) to drive gene transcription of VEGF-C [33] and VEGF-D [34], indicating that the CGRP receptor induces lymphangiogenesis by upregulating VEGF family in inflammatory cells [17]. Further, in vitro experiments demonstrated that CGRP suppressed transcription of VEGF-C in $CD4^+$ cells from $RAMP1^{-/-}$ mice, while the expression of VEGF-D remained unchanged. These results suggest that transcriptional factors involved in VEGF-C induction are different between those in VEGF-D in this model. Indeed, signaling pathways of induction of VEGF-C and VEGF-D appears to be different in fibroblasts and cancer cell lines [35,36]. Further investigations are needed to clarify whether RAMP1 signaling in $CD4^+$ cells regulates VEGF-C induction differently from VEGF-D induction, and to identify the transcription factors and signaling proteins involved in RAMP1-mediated expression of VEGF-C and VEGF-D. Additionally, in vitro experiments also showed that CGRP down-regulated VEGF-C expression in $CD4^+$ cells from $RAMP1^{-/-}$ mice, while CGRP up-regulated VEGF-C expression in $CD4^+$ cells from WT mice. These results suggest that CGRP decreased VEGF-C expression in RAMP1-deficient $CD4^+$ cells through CLR independently by CGRP.

In addition to T cells, macrophages are considered important players in pathological lymphangiogenesis [37]. Indeed, accumulated macrophages play a role in lymphangiogenesis in the diaphragm [20,22]. Depleting macrophages using clodronate liposomes attenuates LPS-induced inflammatory lymphangiogenesis in the diaphragm [22]. The current study shows that RAMP1 signaling in $CD11b^+$ macrophages elicits lymphangiogenesis, a process associated with expression of VEGF-C and VEGF-D. However, excessive accumulation of macrophages in inflamed diaphragm tissues of $RAMP1^{-/-}$ mice was not associated with increased lymphangiogenesis. Consistent with this, we previously reported that blockade of RAMP1 signaling increases the number of macrophages in secondary edema in mouse tails, which is associated with suppressed lymphangiogenesis [18]. The data also suggest that RAMP1 signaling prevents excessive accumulation of macrophages. We also showed that inflammatory-like macrophages suppress lymphangiogenesis [38,39], and that RAMP1 deficiency recruits inflammatory-like macrophages to inflamed tissues [11,18]. The results of the present study also indicate that genes associated with the pro-inflammatory macrophage phenotype were upregulated in $RAMP1^{-/-}$ mice, and that genes associated with the reparative macrophage phenotype were downregulated. Taken together, these data suggest that RAMP1 signaling inhibits excessive infiltration by inflammatory macrophages, and that RAMP1 signaling in recruited macrophages plays a role in lymphangiogenesis during inflammation.

In the current studies, lymphatic vessel markers including LYVE-1, Prox-1, and VEGFR3 in the

diaphragm tissues were down-regulated in RAMP1$^{-/-}$ mice. Because macrophages also express these lymphatic markers, these results suggest that macrophages in RAMP1$^{-/-}$ mice lower the expression of lymphatic markers. The other possibility is that RAMP1 deficient macrophages failed to upregulate VEGF-C, which resulted in down-regulation of LYVE-1, Prox-1, and VEGFR3. These observations suggest that RAMP1 signaling in macrophages plays a role in enhancement of lymphatic vessel markers.

To further understand the role of RAMP1 signaling in macrophages, we induced peritonitis in chimeric mice. The current study shows that BM-derived macrophages expressing RAMP1 promote lymphangiogenesis. Although RAMP1 signaling enhances VEGF-C expression by BM macrophages *in vitro*, it did not affect expression of VEGF-D, which is consistent with our previous results showing that RAMP1 signaling in macrophages facilitates lymphangiogenesis during the course of wound healing via production of VEGF-C by macrophages [17]. These results suggest that RAMP1 signaling in BM-derived macrophages facilitates formation of lymphatic vessels by recruiting repair macrophages via VEGF-C.

It is known that RAMP1$^{-/-}$ mice exhibit hypertension as previously reported [10]. Hypertension would induce endothelial damage, leading to promoting inflammatory activation of endothelial cells and recruitment of inflammatory cells [40]. Altered mechanical forces in hypertension stimulate the endothelium, leading to inflammatory cell recruitment [41]. These findings suggest confounding effects of hypertension on inflammatory cell recruitment to the diaphragmatic lymphatic system. Future studies would assess whether hypertension in RAMP1$^{-/-}$ mice promotes accumulation of inflammatory cells during inflammation.

The function of diaphragmatic lymphatics is to drain peritoneal fluid [19,20]. Functional activation of lymphangiogenesis in the diaphragm may contribute to reducing ascites in pathological conditions such as liver disease. Our data indicate that RAMP1 signaling-dependent lymphangiogenesis in the diaphragm in response to inflammation increases the drainage of peritoneal fluid, together with transport to the mediastinal lymph nodes. In addition, our previous studies show that RAMP1 signaling during skin wound healing promotes fluid drainage through newly formed lymphatic vessels, as evidenced by the movement of fluorescent dye injected subcutaneously into skin wounds [17]. These data indicate that RAMP1 signaling is important for drainage of interstitial fluids through newly developed lymphatic vessels during inflammation.

5. Conclusion

The findings of the current study suggest that lymphangiogenesis in diaphragm tissues during inflammation, together with increased drainage of peritoneal fluid, is medicated by endogenous CGRP/RAMP1 signaling. Inflammation-associated lymphangiogenesis in diaphragm tissues may contribute to draining debris from inflamed tissues. Development of a selective agonist that targets RAMP1 signaling will provide a therapeutic option for patients with peritoneal inflammation.

6. Acknowledgments

We thank Michiko Ogino, Kyoko Yoshikawa and Keisuke Tsuru for technical assistance. We also thank F. Otaka, K. Hattori, M. Honda, A. Ito, K. Yoshino for our lab members.

7. References

1. Wimalawansa SJ. Calcitonin gene-related peptide and its receptors: molecular genetics, physiology, pathophysiology, and therapeutic potentials. *Endocr Rev* 1996;17:533-585.

2. Poyner DR, Sexton PM, Marshall I, Smith DM, Quirion R, Born W, et al. International Union of Pharmacology. XXXII. The mammalian calcitonin gene-related peptides, adrenomedullin, amylin, and calcitonin receptors. *Pharmacol Rev*. 2002; 54: 233-246.

3. Hay DL, Christopoulos G, Christopoulos A, Poyner DR, Sexton PM. Pharmacological discrimination of calcitonin receptor: receptor activity-modifying protein complexes. *Molecular Pharmacology* 2005;67:1655-1665.

4. Kuwasako K, Cao YN, Nagoshi Y, Tsuruda T, Kitamura K, Eto T. Characterization of the human calcitonin gene-related peptide receptor subtypes associated with receptor activity-modifying proteins. *Mol Pharmacol* 2004; 65: 207-213.

5. McLatchie LM, Fraser NJ, Main MJ, Wise A, Brown J, Thompson N, et al. RAMPs regulate the transport and ligand specificity of the calcitonin-receptor-like receptor. *Nature* 1998;393:333–339.

6. Zhang Z, Dickerson IM, Russo AF. Calcitonin gene-related peptide receptor activation by receptor activity-modifying protein-1 gene transfer to vascular smooth muscle cells. *Endocrinology* 2006;147:1932–1940

7. Zhang Z, Winborn CS, Marquez de Prado B, Russo AF. Sensitization of calcitonin gene-related peptide receptors by receptor activity-modifying protein-1 in the trigeminal ganglion. *J. Neurosci.* 2007;27: 2693–2703

8. Hay DL, Pioszak AA. Receptor Activity-Modifying Proteins (RAMPs): New Insights and Roles. *Annu Rev Pharmacol Toxicol.* 2016;56:469-87.

9. Jung WC, Levesque JP, Ruitenberg MJ. It takes nerve to fight back: The significance of neural innervation of the bone marrow and spleen for immune function. *Semin Cell Dev Biol.* 2017; 61: 60-70.

10. Tsujikawa K, Yayama K, Hayashi T, Matsushita H, Yamaguchi T, Shigeno T, et al. Hypertension and dysregulated proinflammatory cytokine production in receptor activity-modifying protein 1-deficient mice. *Proc Natl Acad Sci U S A.* 2007; 104: 16702-16707.

11. Kawashima-Takeda N, Ito Y, Nishizawa N, Kawashima R, Tanaka K, Tsujikawa K, et al. RAMP1 suppresses mucosal injury from dextran sodium sulfate-induced colitis in mice. *J Gastroenterol Hepatol.* 2017 ;32: 809-818.

12. Inoue T, Ito Y, Nishizwa N, Eshima K, Kojo K, Otaka F, et al. RAMP1 in Kupffer cells is a critical regulator in immune-mediated hepatitis. *PLoS One.* 2018; 13 :e0200432.

13. Huggenberger R, Siddiqui SS, Brander D, Ullmann S, Zimmermann K, Antsiferova M, et al. An important role of lymphatic vessel activation in limiting acute inflammation. *Blood.* 2011 ;117: 4667–4678.

14. Kim H, Kataru RP, Koh GY. Inflammation-associated lymphangiogenesis: a double-edged sword? *J Clin Invest.* 2014; 124: 936–942.

15. Kataru RP, Jung K, Jang C, Yang H, Schwendener RA, Baik JE, et al. Critical role of CD11b+ macrophages and VEGF in inflammatory lymphangiogenesis, antigen clearance, and inflammation resolution. *Blood.* 2009;113:5650–5659.

16. Alitalo K. The lymphatic vasculature in disease. *Nat Med.* 2011;17:1371–1380.

17. Kurashige C, Hosono K, Matsuda H, Tsujikawa K, Okamoto H, Majima M. Roles of receptor activity-modifying protein 1 in angiogenesis and lymphangiogenesis during skin wound healing in mice. *FASEB J.* 2014 ;28 :1237-1247.

18. Mishima T, Ito Y, Nishizawa N, Amano H, Tsujikawa K, Miyaji K, et al. RAMP1 signaling improves lymphedema and promotes lymphangiogenesis in mice. *J Surg Res*. 2017; 219: 50-60.

19. Shibata SJ, Hiramatsu Y, Kaseda M, Chosa M, Ichihara N, Amasaki H, et al. The time course of lymph drainage from the peritoneal cavity in beagle dogs. *J Vet Med Sci* 2006; 68: 1143–1147.

20. Matsuda H, Hosono K, Tsuru S, Kurashige C, Sekiguchi K, Akira S, et al. Roles of mPGES-1, an inducible prostaglandin E synthase in enhancement of LPS-induced lymphangiogenesis in a mouse peritonitis model. *Life Sci.* 2015; 142: 1-7.

21. Ochsenbein AM, Karaman S, Proulx ST, Goldmann R, Chittazhathu J, Dasargyri A, et al. Regulation of lymphangiogenesis in the diaphragm by macrophages and VEGFR-3 signaling. *Angiogenesis*. 2016;19: 513-524.

22. Kim KE, Koh YJ, Jeon BH, Jang C, Han J, Kataru RP, et al. Role of CD11b+ macrophages in intraperitoneal lipopolysaccharide-induced aberrant lymphangiogenesis and lymphatic function in the diaphragm. *Am J Pathol* 2009; 175: 1733–1745.

23 Kawai S, Takagi Y, Kaneko S, Kurosawa T. Effect of three types of mixed anesthetic agents alternate to ketamine in mice. *Exp Anim* 2011;60: 481-487.

24. Nishizawa N, Ito Y, Eshima K, Ohkubo H, Kojo K, Inoue T, et al. Inhibition of microsomal prostaglandin E synthase-1 facilitates liver repair after hepatic injury in mice. *J Hepatol*. 2018; 69: 110-120.

25. Mikami N, Matsushita H, Kato T, Kawasaki R, Sawazaki T, Kishimoto T, et al. Calcitonin gene-related peptide is an important regulator of cutaneous immunity: effect on dendritic cell and T cell functions. *J Immunol*. 2011; 186: 6886-6893.

26. Altmayr F, Jusek G, Holzmann B. The neuropeptide calcitonin gene-related peptide causes repression of tumor necrosis factor-alpha transcription and suppression of ATF-2 promoter recruitment in Toll-like receptor-stimulated dendritic cells. *J Biol Chem*. 2010; 285: 3525-3231.

27. Ohno T, Hattori Y, Komine R, Ae T, Mizuguchi S, Arai K, et al. Roles of calcitonin gene-related peptide in maintenance of gastric mucosal integrity and in enhancement of ulcer healing and angiogenesis. *Gastroenterology*. 2008; 134: 215-225.

28. Toda M, Suzuki T, Hosono K, Hayashi I, Hashiba S, Onuma Y, et al. Neuronal system-dependent facilitation of tumor angiogenesis and tumor growth by calcitonin gene-related peptide. *Proc Natl Acad Sci U S A*. 2008; 105: 13550-13555.

29. Mishima T, Ito Y, Hosono K, Tamura Y, Uchida Y, Hirata M, Suzsuki T, Amano H, Kato S, Kurihara Y, Kurihara H, Hayashi I, Watanabe M, Majima M. Calcitonin gene-related peptide facilitates revascularization during hindlimb ischemia in mice. *Am J Physiol Heart Circ Physiol.* 2011; 300: H431-439.

30. Ogata F, Fujiu K, Matsumoto S, Nakayama Y, Shibata M, Oike Y, et al. Excess Lymphangiogenesis Cooperatively Induced by Macrophages and CD4(+) T Cells Drives the Pathogenesis of Lymphedema. *J Invest Dermatol*. 2016; 136: 706-714.

31. Majima M, Ito Y, Hosono K, Amano H. CGRP/CGRP Receptor Antibodies: Potential Adverse Effects Due to Blockade of Neovascularization? *Trends Pharmacol Sci*. 2019 ;40:11-21.

32. Amano H, Ando K, Minamida S, Hayashi I, Ogino M, Yamashina S, et al. Adenylate cyclase/protein kinase A sig-naling pathway enhances angiogenesis through induction of vascular endothelial growth factor in vivo. *Jpn. J. Pharmacol*. 2001; 87: 181–188.

33. Singh NK, Kotla S, Kumar R, Rao GN. Protein Mediates Pathological Retinal Neovascularization via Modulating DLL4-NOTCH1 Signaling. *EBioMedicine*. 2015; 2:1767-1784.

34. Schäfer G, Wissmann C, Hertel J, Lunyak V, Höcker M. Regulation of vascular endothelial growth factor D by orphan receptors hepatocyte nuclear factor-4 alpha and chicken ovalbumin upstream promoter transcription factors 1 and 2. *Cancer Res*. 2008;68:457-466.

35. Orlandini M, Marconcini L, Ferruzzi R, Oliviero S. Identification of a c-fos-induced gene that is related to the platelet-derived growth factor/vascular endothelial growth. *Proc. Natl. Acad. Sci. USA* 1996;93: 11675–11680.

36. Hong H, Jiang L, Lin Y, He C, Zhu G, Du Q, et al. TNF-alpha promotes lymphangiogenesis and

lymphatic metastasis of gallbladder cancer through the ERK1/2/AP-1/VEGF-D pathway. *BMC Cancer.* 2016;16:240.

37. Harvey NL, Gordon EJ. Deciphering the roles of macrophages in developmental and inflammation stimulated lymphangiogenesis. *Vasc Cell* 2012; 4: 15-21.

38. Okizaki S, Ito Y, Hosono K, Oba K, Ohkubo H, Kojo K, et al. Vascular Endothelial Growth Factor Receptor Type 1 Signaling Prevents Delayed Wound Healing in Diabetes by Attenuating the Production of IL-1β by Recruited Macrophages. *Am J Pathol.* 2016; 186: 1481-1498.

39. Hosono K, Isonaka R, Kawakami T, Narumiya S, Majima M. Signaling of Prostaglandin E Receptors, EP3 and EP4 Facilitates Wound Healing and Lymphangiogenesis with Enhanced Recruitment of M2 Macrophages in Mice. *PLoS One*. 2016; 11:e0162532.

40. Pauletto P, Rattazzi M. Inflammation and hypertension: the search for a link. *Nephrol Dial Transplant*. 2006; 21: 850-853.

41. Loperena R, Van Beusecum JP, Itani HA, Engel N, Laroumanie F, Xiao L, et al. Hypertension and increased endothelial mechanical stretch promote monocyte differentiation and activation: roles of STAT3, interleukin 6 and hydrogen peroxide. *Cardiovasc Res.* 2018; 114: 1547-1563.

8. Figure legends

Fig. 1 Deficient RAMP1 signaling suppresses lymphangiogenesis and pro-lymphangiogenic factors in diaphragm tissues during inflammation.

a Representative images showing lymphatic vessels in whole mount diaphragm tissue stained with antibodies specific for Lyve-1 (green) at 7 days post-injection of LPS into the peritoneal cavity of WT and RAMP1$^{-/-}$ mice. Scale bars, 200 μm. **b** The percentage lymphatic vessel area (LVA%) in whole mount diaphragm tissue from WT and RAMP1$^{-/-}$ mice. Data are expressed as the mean ± SEM (4–6 mice per group). *$p < 0.05$. **c-e** Expression of mRNA encoding Lyve-1, VEGFR3, and Prox-1 in diaphragm tissue from WT and RAMP1$^{-/-}$ mice. Data are expressed as the mean ± SEM (4–6 mice per group). *$p < 0.05$. **f, g** Expression of mRNA encoding VEGF-C and VEGF-D in diaphragm tissue from WT and RAMP1$^{-/-}$ mice. Data are expressed as the mean ± SEM (4–6 mice per group). *$p < 0.05$.

Fig. 2 Accumulation of CD4$^+$ and CD11b$^+$ cells in diaphragm tissue after LPS injection.

a Representative images showing immunofluorescence staining of CD4 (red) or CD11b (green) in

diaphragm tissue from WT and RAMP1$^{-/-}$ mice at Day 3. Nuclei are stained by DAPI (blue). Scale bars, 100 μm. **b** Number of CD4^{+} cells after LPS injection. Data are expressed as the mean ± SD (4–6 mice per group). *$p < 0.05$. **c** Number of CD11b^{+} cells after LPS injection. Data are expressed as the mean ± SD (4–6 mice per group). *$p < 0.05$. **d** Representative images showing dual immunofluorescence labeling of CD4 (red) and VEGF-C (green) or VEGF-D (red) in tissue from WT mice at Day 3. Nuclei are stained by DAPI (blue). Merged signals are yellow. Scale bars, 50 μm. **e** Representative images of diaphragm tissue from WT mice showing immunofluorescence staining of tissues for CD11b (red) and VEGF-C (green) or VEGF-D (red) (Day 3). Nuclei are stained by DAPI (blue). Merged signals are yellow. Scale bars, 50 μm.

Fig. 3 Involvement of CD4^{+} T cells in lymphangiogenesis during inflammation.

a Diaphragms from WT mice treated with control IgG or anti-CD4 antibodies were stained with Lyve-1 (green). Scale bars, 200 μm. **b** Effects of anti-CD4 antibodies on LVA% at Day 7. Data are expressed as the mean ± SD (4 mice per group). *$p < 0.05$. **c, d** Expression of mRNA encoding VEGF-C and VEGF-D in the diaphragm tissues from WT and RAMP1$^{-/-}$ mice treated with control IgG or anti-CD4 antibodies (Day 5). Data are expressed as the mean ± SD (6 mice per group). *$p < 0.05$. **e, f** Amounts of VEGF-C and VEGF-D mRNA expressed by splenic CD4^{+} T cells isolated from WT and RAMP1$^{-/-}$ mice. Isolated splenic CD4^{+} T cells were stimulated with CGRP (10 nM) with or without LPS (100 ng/ml) for 3 h. Splenic CD4^{+} T cells were isolated by magnetic-activated cell sorting. Data are expressed as the mean ± SD (4–6 mice per group).

Fig. 4 Effect of RAMP1 expression in macrophages on expression of genes associated with inflammation.

a, b Expression of mRNA encoding genes associated with a pro-inflammatory macrophage phenotype (A) and with a reparative phenotype (B) in diaphragm tissues at Days 0 and 3. Data are expressed as the mean ± SD (4 mice per group). *$p < 0.05$. **c, d** Expression of mRNA encoding chemokines CCL2 and CCL5 in the diaphragm. Data are expressed as the mean ± SD (4 mice per group). *$p < 0.05$.

Fig. 5 Effects of RAMP1 expression in bone marrow macrophages on genes associated with inflammation and pro-lymphangiogenic factors.

(a-d) Expression of mRNA encoding TNFα, MR, VEGF-C, and VEGF-D in cultured BM-derived macrophages from WT and RAMP1$^{-/-}$ mice stimulated with CGRP. Data are expressed as the mean ± SD (4–6 mice per group). *$p < 0.05$.

Fig. 6 Loss of RAMP1 results in impaired drainage of peritoneal fluid.

a Residual amounts of FITC-dextran were assessed 10 min after injection into the peritoneal cavity of

WT and RAMP1$^{-/-}$ mice treated with LPS or vehicle (saline) at Day 7. Data are expressed as the mean ± SD (6 mice per group). *$p < 0.05$. **b** Photographs showing the right mediastinal lymph nodes in the pleural cavity after injection of FITC-dextran into peritoneal cavity of WT and RAMP1$^{-/-}$ mice. FITC-dextran was drained through the lymphatic vessels from the peritoneal cavity, and flowed into the mediastinal lymph nodes. **c** Residual amounts of FITC-dextran in the right mediastinal lymph nodes from WT and RAMP1$^{-/-}$ mice treated with LPS or vehicle (saline) at Day 7. The right mediastinal lymph nodes were removed immediately after collection of peritoneal fluid. Data are expressed as the mean ± SD (6 mice per group). *$p < 0.05$.

Supplementary Fig. 1 Time course of lymphatic vessel formation during inflammation in the diaphragm.

(A) Lymphatic vessels in whole mount diaphragm tissue were stained with antibodies specific for Lyve-1 (green) 5 days post-injection of LPS or vehicle (PBS) into the peritoneal cavity of WT mice. Scale bar, 200 μm. (B) Percentage lymphatic vessel area (LVA%) in whole mount diaphragm tissue. Data are expressed as the mean ± SD (4–6 mice per group). *$p < 0.05$.

Supplementary Fig. 2 Expression of RAMP1 in the cervical dorsal root ganglions and diaphragm tissue.

(A–C) Expression of mRNA encoding pro-CGRP (A), CGRP (B), and RAMP1 (C) in dorsal root ganglion tissues from WT and RAMP1$^{-/-}$ mice at Day 0 (day at the beginning of the experiment just prior to the first LPS administration). Data are expressed as the mean ± SD (4–6 mice per group). *$p < 0.05$. (D) Double immunostaining of diaphragm sections from WT mice at Day 0 and Day 7 (7 days after the start of the first LPS administration) with antibodies specific for RAMP-1 (green), Lyve-1 (red) (E,F). Scale bars, 50 μm. Double immunostaining of diaphragm sections from WT mice at Day 3 with antibodies specific for RAMP-1 (green) and CD4 (red) (E), or CD11b (red) (F). Cell nuclei were stained with DAPI (blue). Double-positive cells are yellow. Scale bars, 50 μm.

Supplementary Figure 3. Effect of anti-CD4 antibodies on CD4$^+$ cells in the spleen and blood.

(A) Representative flow cytometric dot plots analysis for CD4$^+$ T cells (CD3^{high}/CD4^{high}) in the spleen from WT and RAMP1$^{-/-}$ mice treated with control IgG or anti-CD4 antibodies. CD4 antibodies were administered one day before. (B,C) Flow cytometry analysis of the percentage of CD3^{high}/CD4^{high} cells in the spleen (B) and blood (C) after CD4 antibody or control IgG. Data are expressed as the mean ± SD of 3-4 mice per group. *$p < 0.05$

Supplementary Figure 4. Bone marrow (BM)-derived macrophages expressing RAMP1 suppress lymphangiogenesis in diaphragm tissues during inflammation.

(A) Representative images of diaphragms from WT→WT mice and RAMP1$^{-/-}$→WT mice stained with Lyve-1 (green). Scale bars, 200 μm. (B) LVA% in diaphragm tissue from WT→WT mice and RAMP1$^{-/-}$→WT mice on Day 7.

Data are expressed as the mean ± SD (3–5 mice per group). *$p < 0.05$. (C, D) Representative images of dual immunofluorescence staining for GFP (green) and CD11b (red) or CD4 (red) in tissue from WT mice receiving BM cells from GFP^+-transgenic WT mice (Day 7). Nuclei are stained by DAPI (blue). Merged signals are yellow. Scale bars, 25 μm.

Supplementary Figure 5. Changes in the intraperitoneal pressure after injection of saline.
Representative charts of the intraperitoneal pressure after injection of saline in LPS-treated WT mice (upper) and $RAMP1^{-/-}$ mice (lower) at Day 7. Changes in the intraperitoneal pressure after injection of saline in LPS-treated WT and $RAMP1^{-/-}$ mice at Day 7. Data are expressed as the mean ± SD (3 mice per group).

Supplementary Table 1.
Primers used for reverse transcription and quantitative PCR.

9. Figure

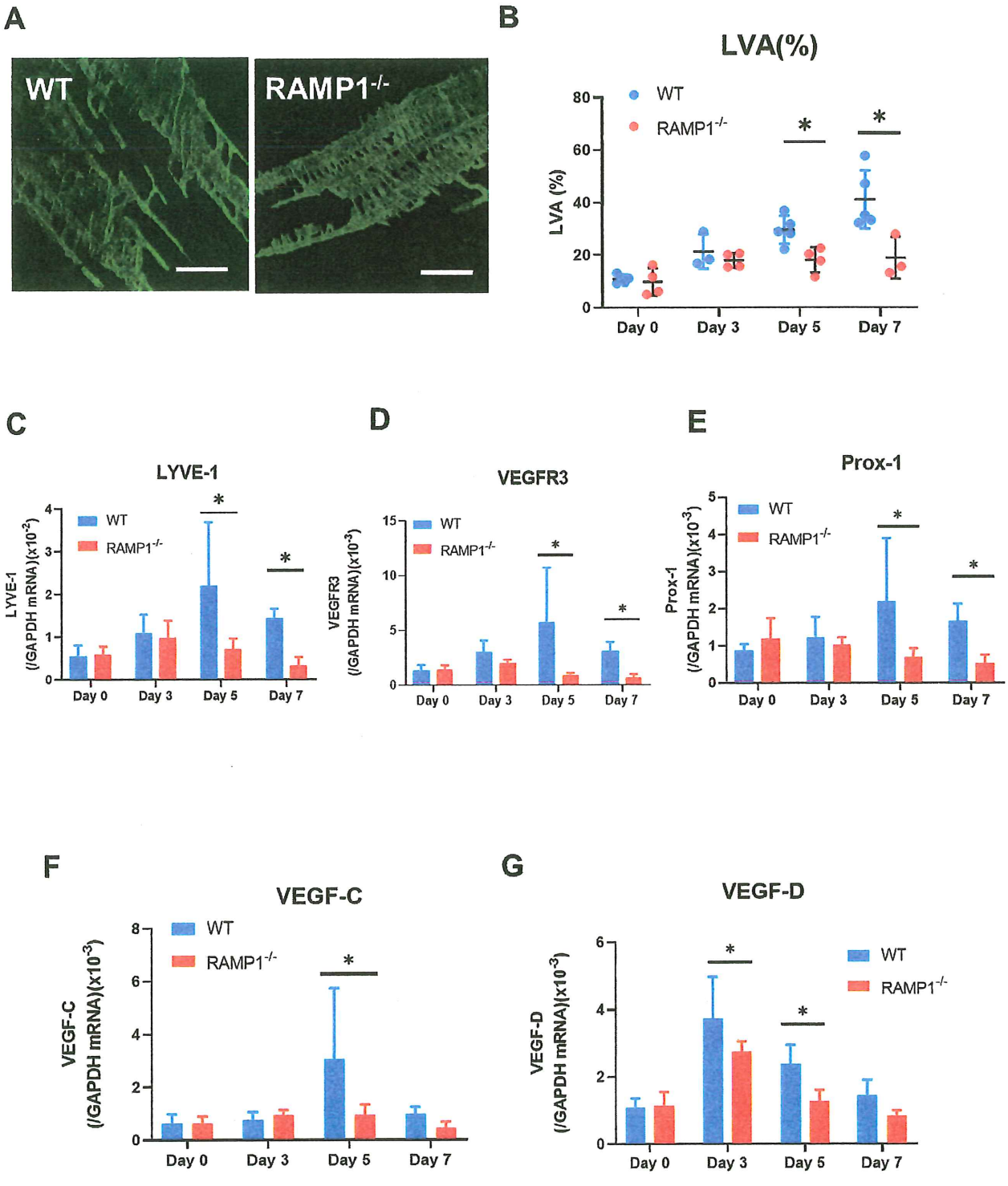
A
WT
RAMP1-/-
B
LVA(%)
WT
RAMP1-/-
LVA (%)
Day 0
Day 3
Day 5
Day 7
C
LYVE-1
LYVE-1 (/GAPDH mRNA)(x10-2)
D
VEGFR3
VEGFR3 (/GAPDH mRNA)(x10-3)
E
Prox-1
Prox-1 (/GAPDH mRNA)(x10-3)
F
VEGF-C
VEGF-C (/GAPDH mRNA)(x10-3)
G
VEGF-D
VEGF-D (/GAPDH mRNA)(x10-3)

Figure 1

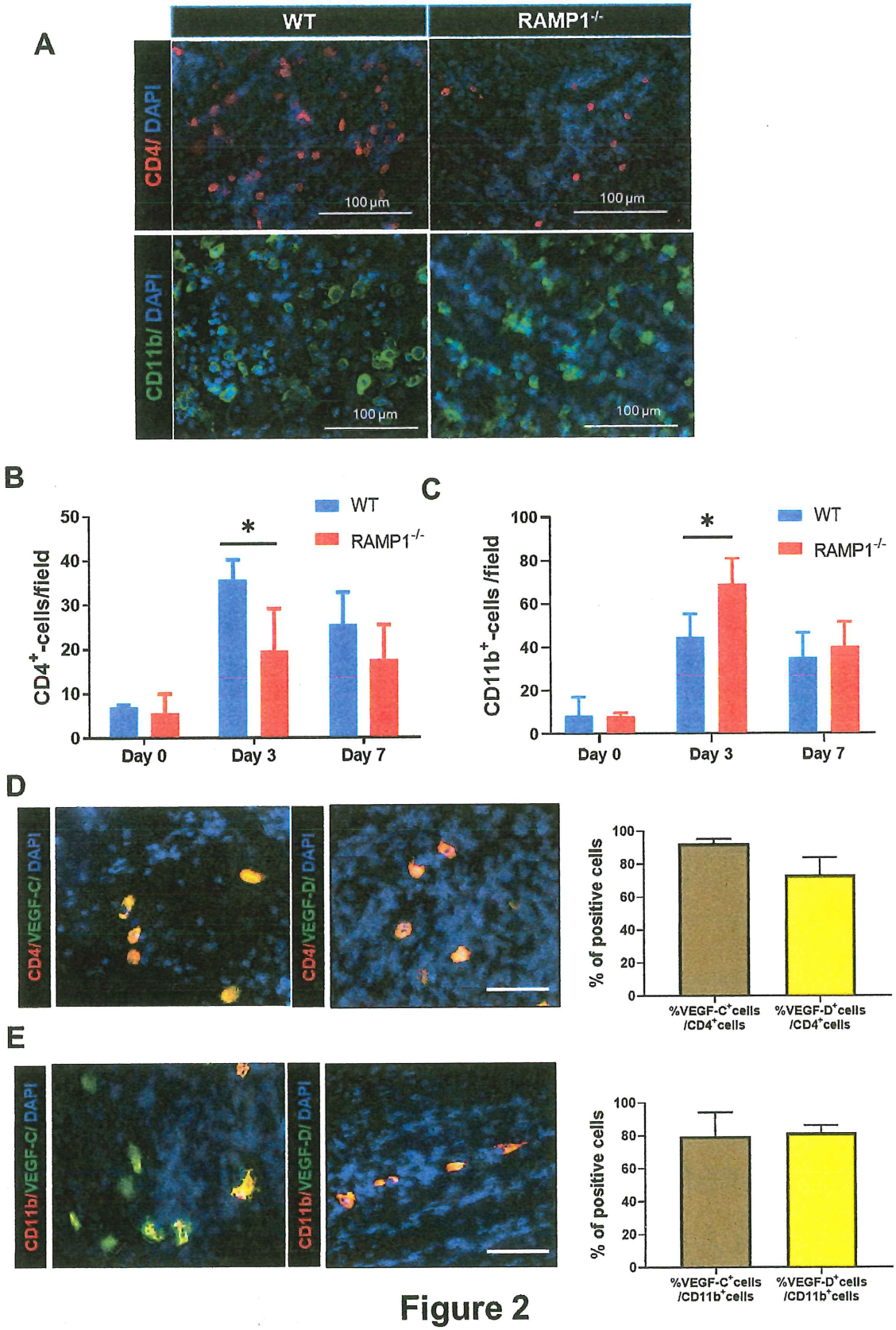
A
WT
RAMP1-/-
CD4/ DAPI
CD11b/ DAPI
100 μm
B
CD4+-cells/field
WT
RAMP1-/-
*
Day 0
Day 3
Day 7
C
CD11b+-cells /field
D
CD4/VEGF-C/ DAPI
CD4/VEGF-D/ DAPI
% of positive cells
%VEGF-C+cells /CD4+cells
%VEGF-D+cells /CD4+cells
E
CD11b/VEGF-C/ DAPI
CD11b/VEGF-D/ DAPI
%VEGF-C+cells /CD11b+cells
%VEGF-D+cells /CD11b+cells

Figure 2

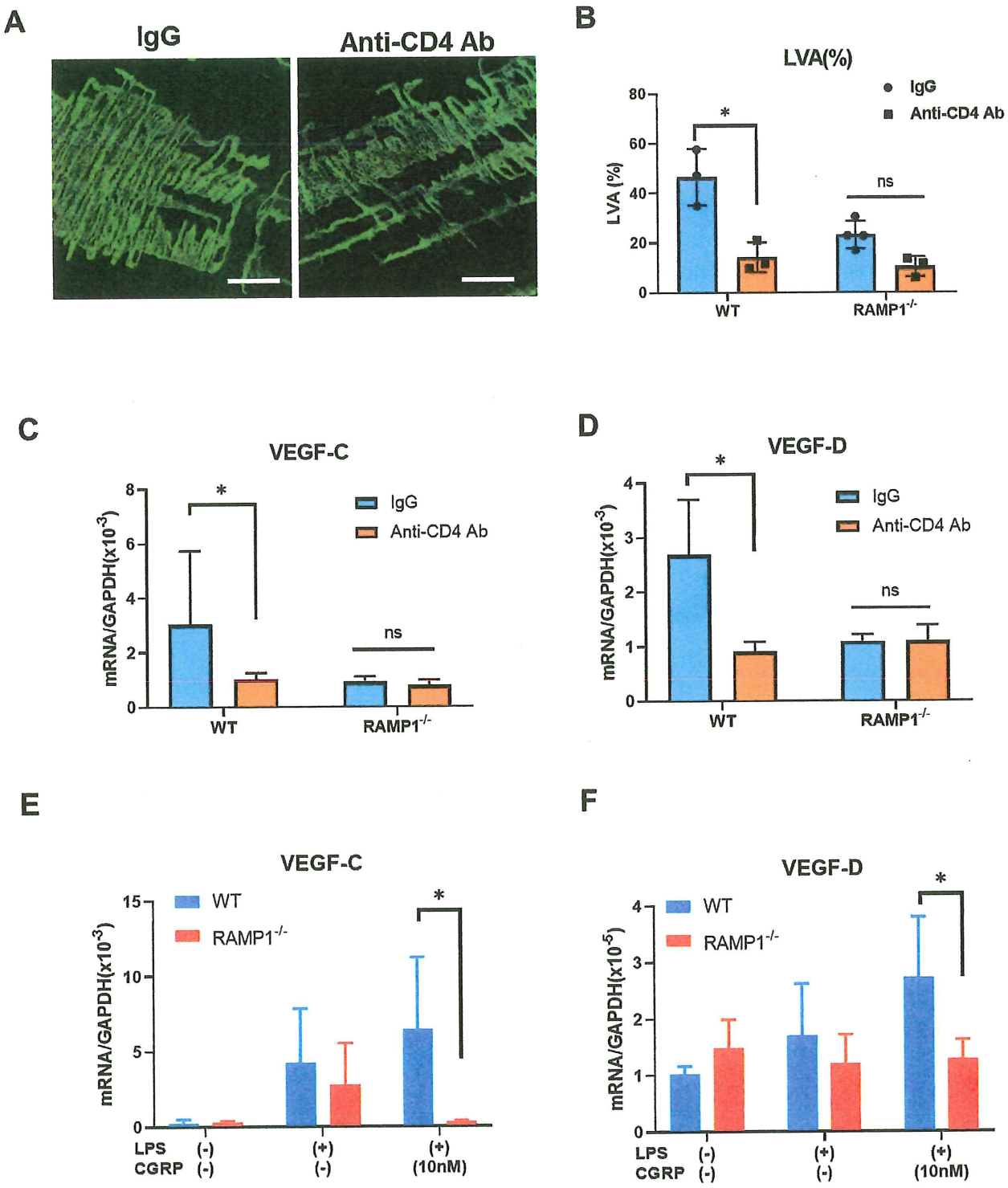
A
IgG
Anti-CD4 Ab
B
LVA(%)
IgG
Anti-CD4 Ab
LVA (%)
80
60
40
20
0
*
ns
WT
RAMP1-/-
C
VEGF-C
mRNA/GAPDH(x10-3)
8
6
4
2
0
*
ns
IgG
Anti-CD4 Ab
WT
RAMP1-/-
D
VEGF-D
mRNA/GAPDH(x10-3)
4
3
2
1
0
*
ns
IgG
Anti-CD4 Ab
WT
RAMP1-/-
E
VEGF-C
mRNA/GAPDH(x10-3)
15
10
5
0
WT
RAMP1-/-
*
LPS (-) (+) (+)
CGRP (-) (-) (10nM)
F
VEGF-D
mRNA/GAPDH(x10-5)
4
3
2
1
0
WT
RAMP1-/-
*
LPS (-) (+) (+)
CGRP (-) (-) (10nM)

Figure 3

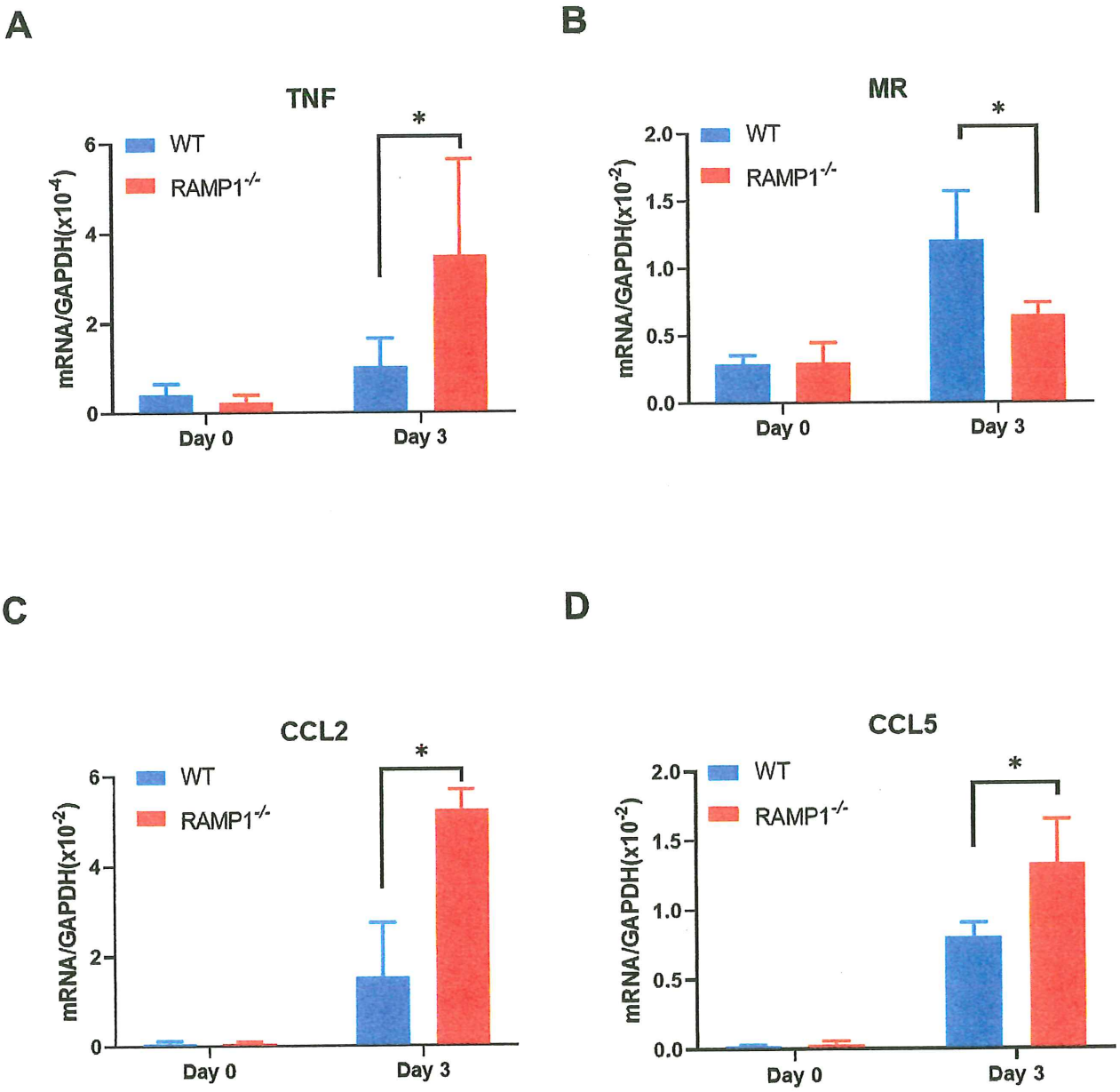
A
TNF
WT
RAMP1-/-
mRNA/GAPDH(x10-4)
6
4
2
0
*
Day 0
Day 3
B
MR
WT
RAMP1-/-
mRNA/GAPDH(x10-2)
2.0
1.5
1.0
0.5
0.0
*
Day 0
Day 3
C
CCL2
WT
RAMP1-/-
mRNA/GAPDH(x10-2)
6
4
2
0
*
Day 0
Day 3
D
CCL5
WT
RAMP1-/-
mRNA/GAPDH(x10-2)
2.0
1.5
1.0
0.5
0.0
*
Day 0
Day 3

Figure 4

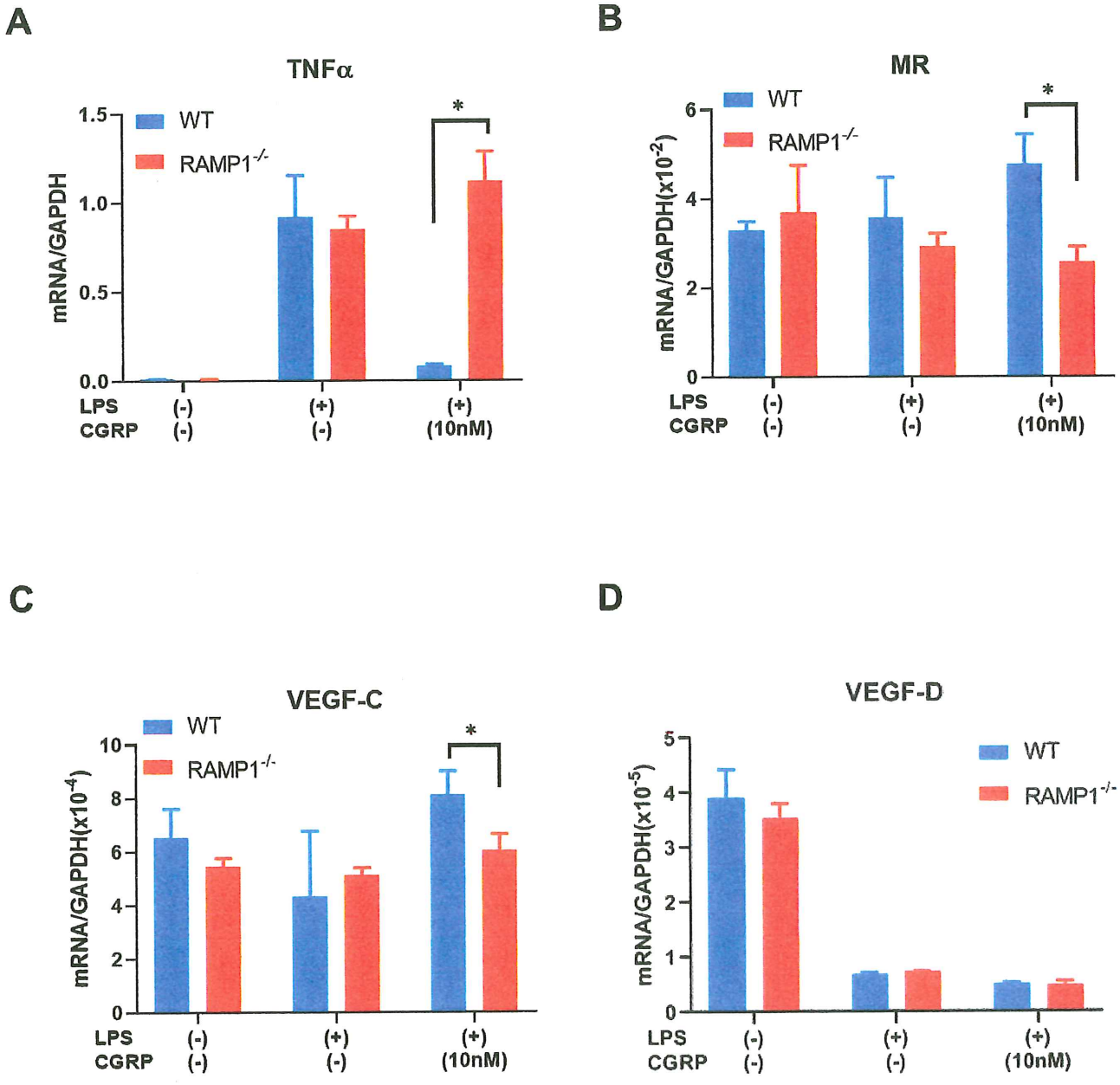
A
TNFα
mRNA/GAPDH
1.5
1.0
0.5
0.0
WT
RAMP1-/-
*
LPS (-) (+) (+)
CGRP (-) (-) (10nM)
B
MR
mRNA/GAPDH(x10-2)
6
4
2
0
WT
RAMP1-/-
*
LPS (-) (+) (+)
CGRP (-) (-) (10nM)
C
VEGF-C
mRNA/GAPDH(x10-4)
10
8
6
4
2
0
WT
RAMP1-/-
*
LPS (-) (+) (+)
CGRP (-) (-) (10nM)
D
VEGF-D
mRNA/GAPDH(x10-5)
5
4
3
2
1
0
WT
RAMP1-/-
LPS (-) (+) (+)
CGRP (-) (-) (10nM)

Figure 5

A

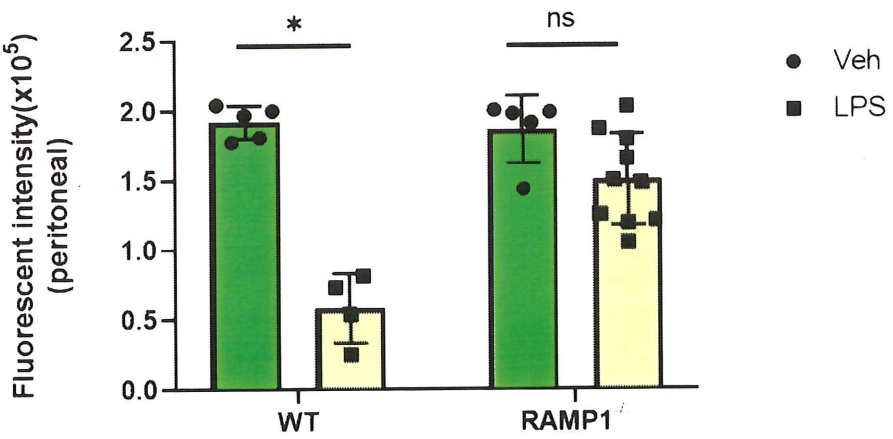
Fluorescent intensity(x10^5)
(peritoneal)
2.5
2.0
1.5
1.0
0.5
0.0
*
ns
WT
RAMP1$^{-/-}$
Veh
LPS

B

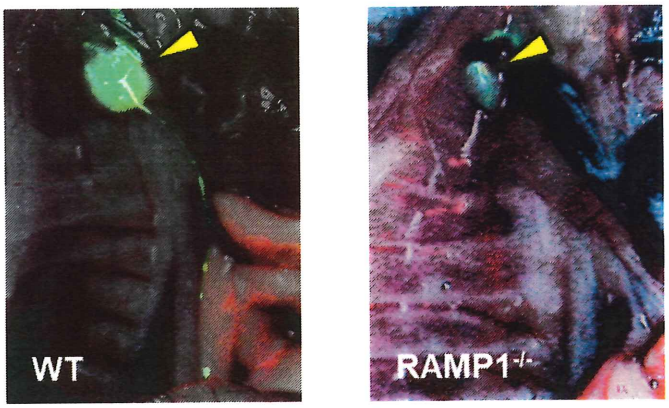
WT
RAMP1$^{-/-}$

C

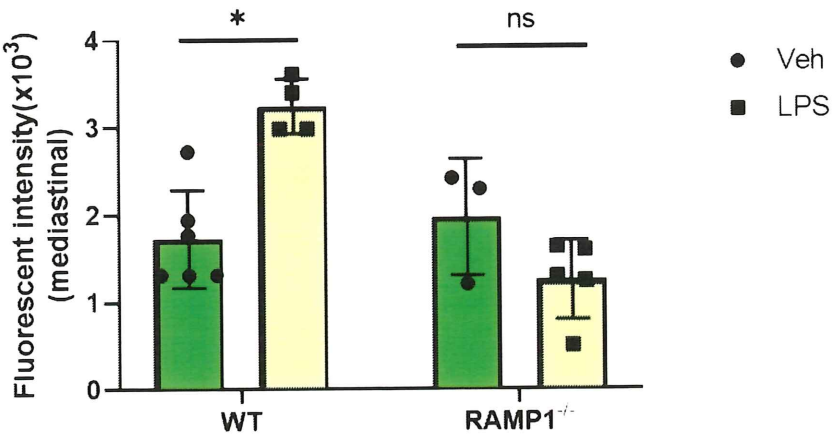
Fluorescent intensity(x10^3)
(mediastinal)
4
3
2
1
0
*
ns
WT
RAMP1$^{-/-}$
Veh
LPS

Figure 6

A

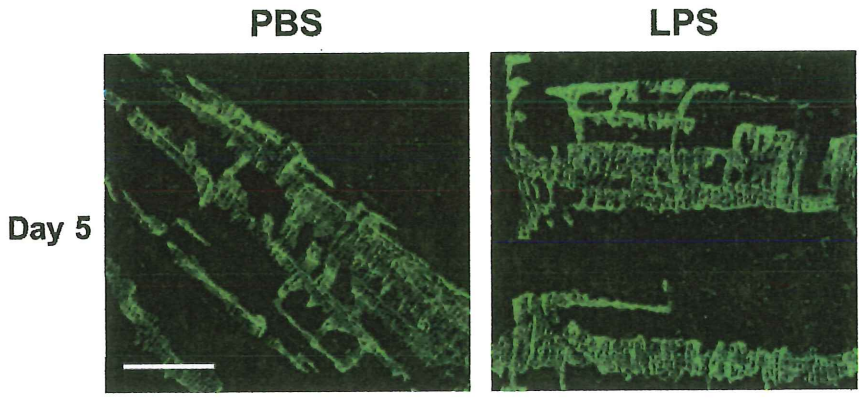

B

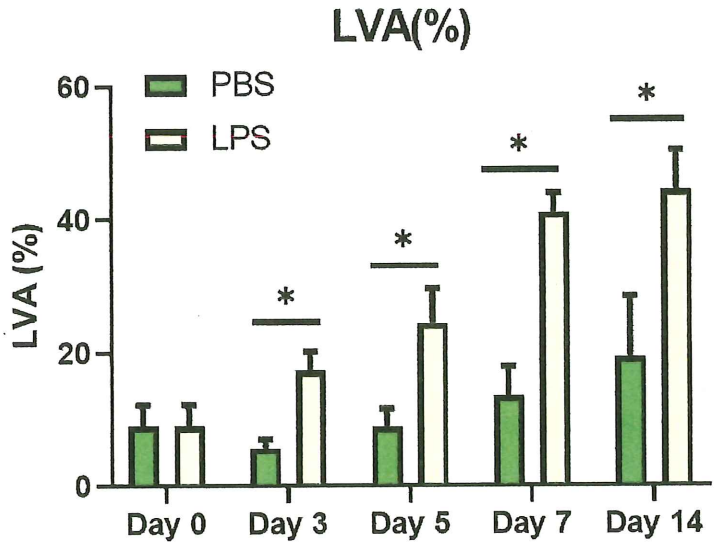

Supplementary Figure 1

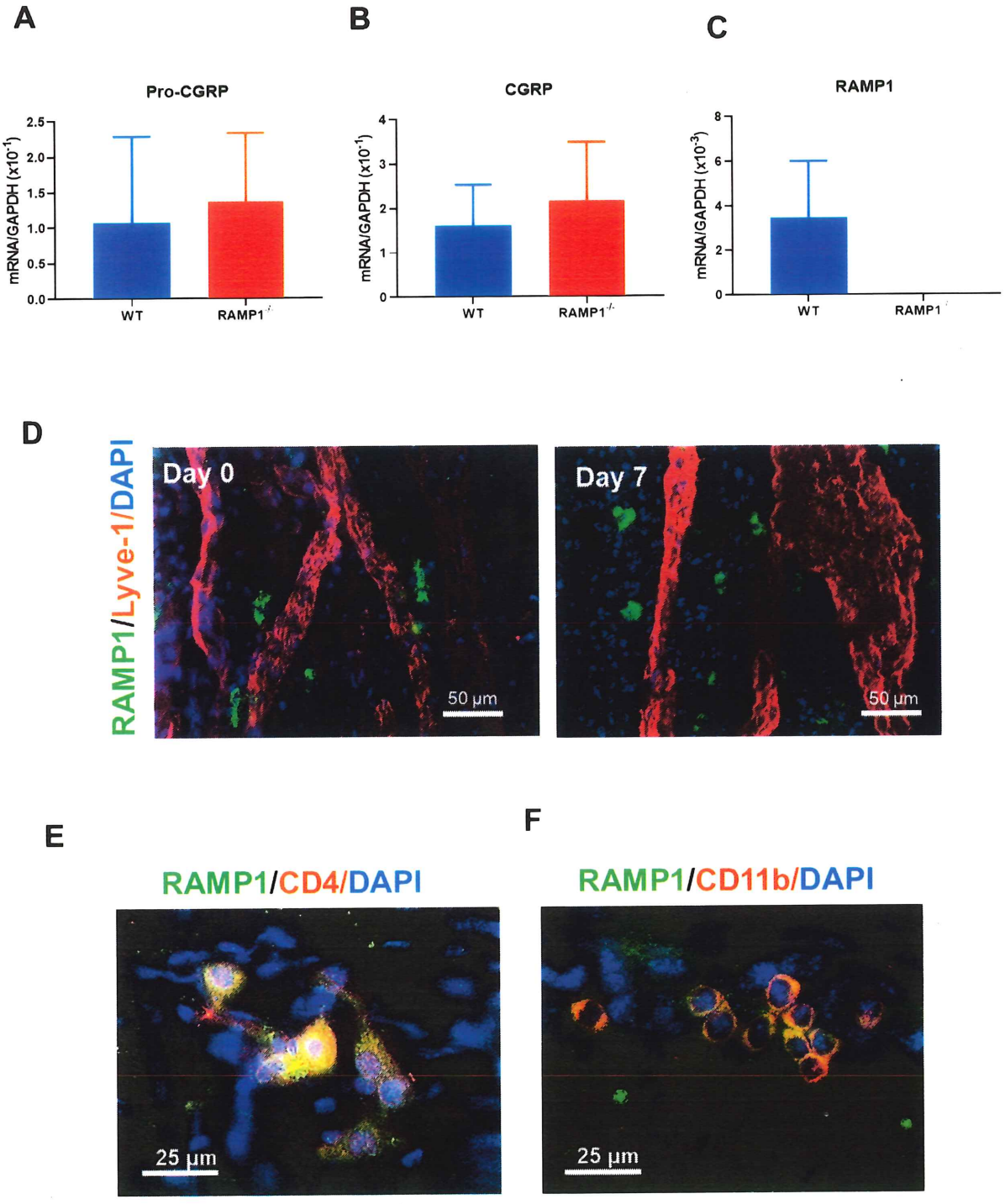

Supplementary Figure 2

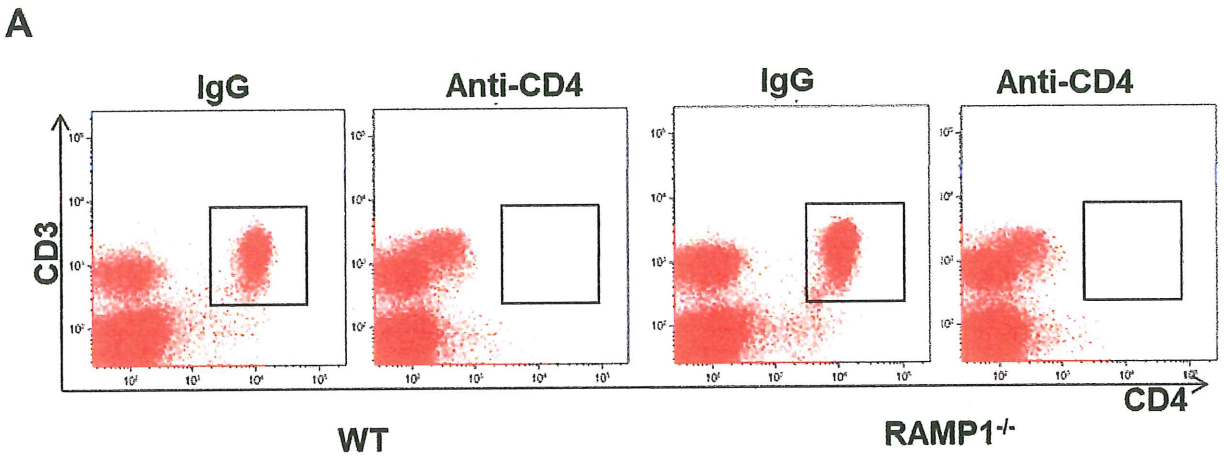

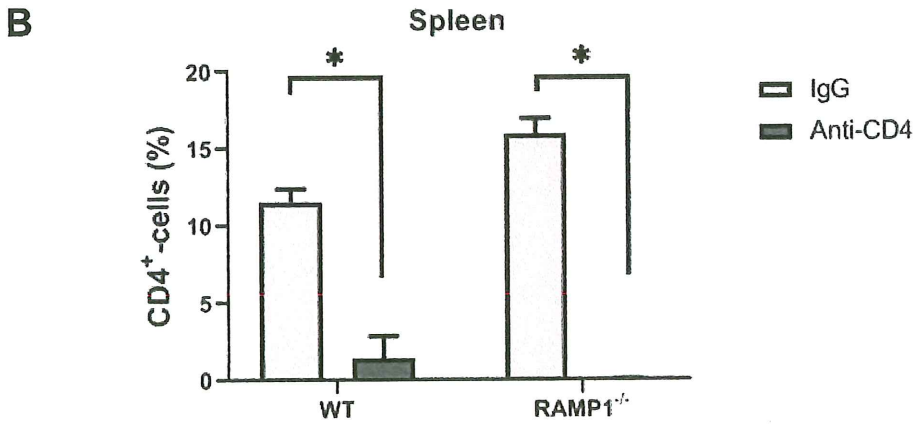

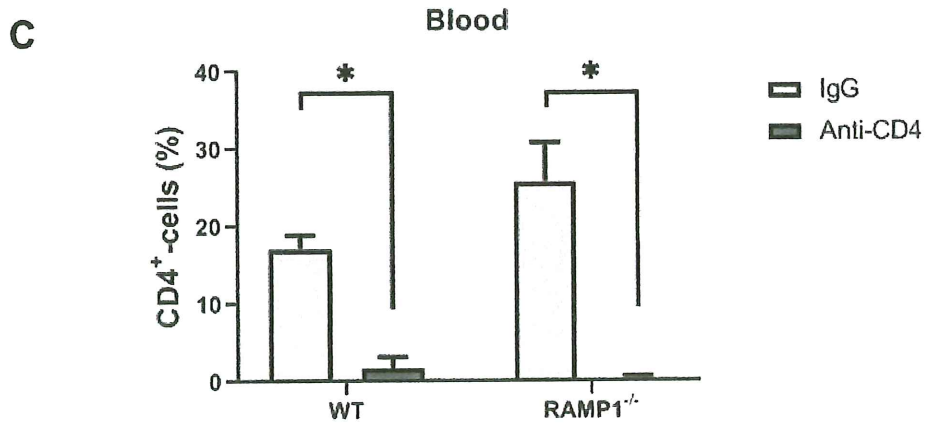

Supplementary Figure 3

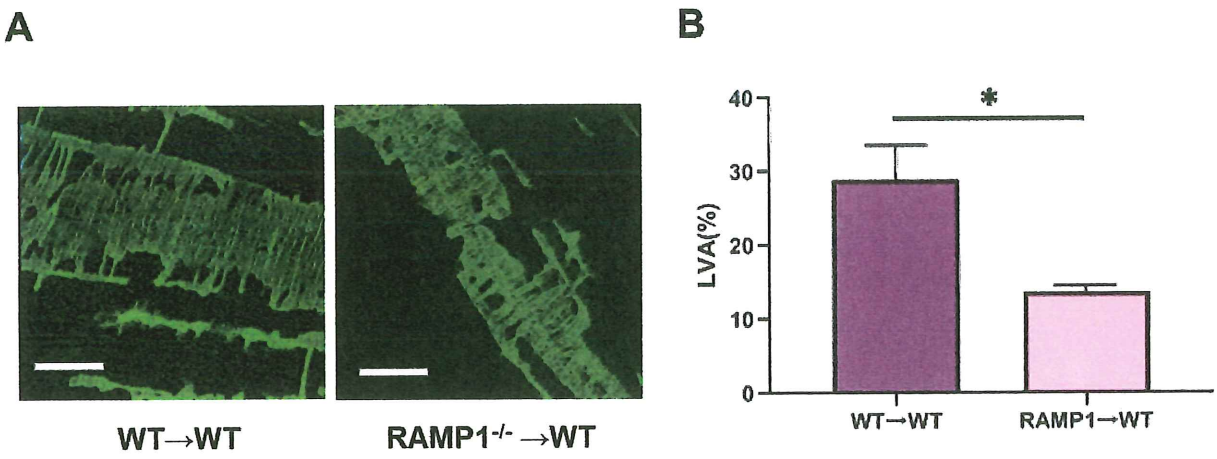

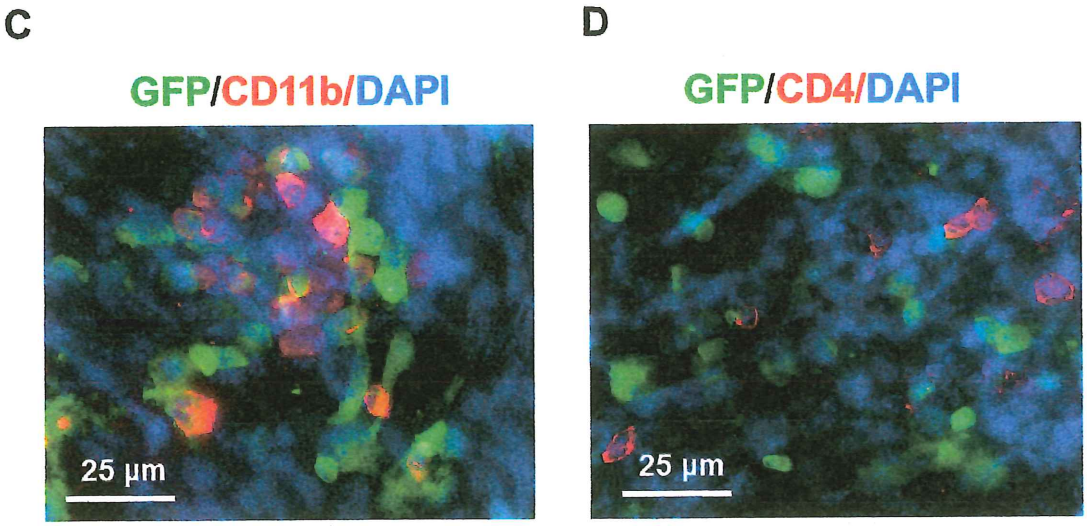

Supplementary Figure 4

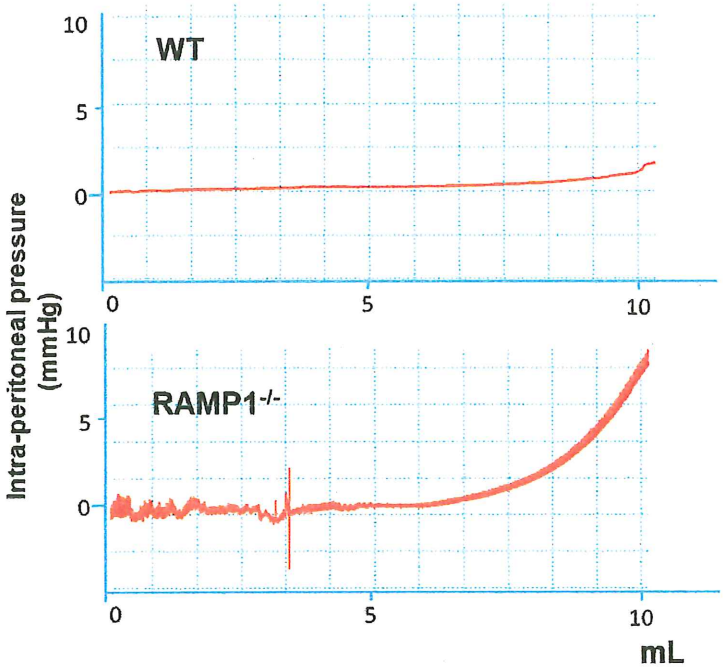

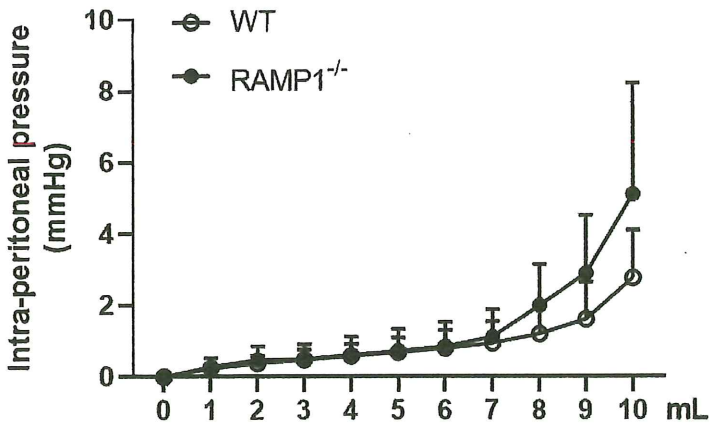

Supplementary Figure 5

Gene	Forward primer sequence (5'–3')	Reverse primer sequence (5'–3')
GAPDH	ACATCAAGAAGGTGGTGAAGC	AAGGTGGAAGAGTGGGAGTTG
LYVE-1	GCTCTCCTCTTCTTTGGTGCT	TGACGTCATCAGCCTTCTCTT
VEGFR-3	CTCTCCAACTTCTTGCGTGTC	GCTTCCAGGTCTCCTCCTATC
Prox-1	GTTCTTTTACACCCGCTACCC	ACTCACGGAAATTGCTGAACC
VEGF-C	TCTGTGTCCAGCGTAGATGAG	GTCCCCTGTCCTGGTATTGAG
VEGF-D	CCTATTGACATGCTGTGGGAT	GTGGGTTCCTGGAGGTAAGAG
Pro-CGRP	CCCCAGAATGAAGGTTACACA	TGTCAAAGGGAGAAGGGTTTT
CGRP	AGGGCTCTAGTGTTCACTGCTC	AGTTGTCCTTCACCACACCTC
RAMP1	CCATCTCTTCATGGTCACTGC	AGCGTCTTCCCAATAGTCTCC
TNFα	TCTTCTCATTCCTGCTTGTGG	GATCTGAGTGTGAGGGTCTGG
MR	TTTGTCCATTGCACTTTGAGG	TGCCAGGTTAAAGCAGACTTG
CCL2	CGGAACCAAATGAGATCAGAA	TTGTGGAAAAGGTAGTGGATG
CCL5	CTGCTGCTTTGCCTACCTCTC	GTGACAAACACGACTGCAAGA